Off-axis electron holography of pseudo-spin-valve thin-film magnetic elements

T. Kasama[a]
Frontier Research System, The Institute of Physical and Chemical Research, Hatoyama, Saitama 350-0395, Japan and Department of Materials Science and Metallurgy, University of Cambridge, Pembroke Street, Cambridge CB2 3QZ, United Kingdom

P. Barpanda
Department of Materials Science and Metallurgy, University of Cambridge, Pembroke Street, Cambridge CB2 3QZ, United Kingdom

R. E. Dunin-Borkowski
Department of Materials Science and Metallurgy, University of Cambridge, Pembroke Street, Cambridge CB2 3QZ, United Kingdom and Frontier Research System, The Institute of Physical and Chemical Research, Hatoyama, Saitama 350-0395, Japan

S. B. Newcomb
Glebe Scientific Limited, Glebe Laboratories, Newport, Co. Tipperary, Ireland

M. R. McCartney
Department of Physics and Astronomy, Arizona State University, Tempe, Arizona 85287-1504

F. J. Castaño and C. A. Ross
Department of Materials Science and Engineering, Massachusetts Institute of Technology, Cambridge, Massachusetts 02139

Magnetic remanent states in a rectangular array of 75×280-nm^2 NiFe/Cu/Co thin-film pseudo-spin-valve elements are studied using off-axis electron holography in the transmission electron microscope (TEM). An approach based on focused ion-beam milling is used to minimize damage to the magnetic properties of the elements during preparation for TEM examination in plan-view geometry. Experimental electron holographic phase images are used to measure the switching fields of the Co and NiFe layers in each of three adjacent elements separately, and comparisons with micromagnetic simulations are used to infer the true magnetic thicknesses and widths of the layers. Demagnetizing fields are included in the discussion of the results, and the possibility that the conclusions may be affected by the procedure used to analyze the holograms is discussed. © *2005 American Institute of Physics*. [DOI: 10.1063/1.1943511]

I. INTRODUCTION

Thin-film magnetic structures are central to the development of spintronic devices such as magnetic random access memories[1,2] and magnetoresistive read heads.[3,4] A typical magnetoresistive multilayer contains a hard (pinned) layer and a soft (free) layer, which are separated by a tunnel barrier or a conductive spacer. The resistance of the structure depends on the relative magnetization directions of the two layers. This effect can be used to sense small magnetic fields (which rotate the magnetization direction of the free layer) or to store a data bit. For the development of spintronic devices, it is important to characterize the switching field distributions of deep-submicron structures. However, most magnetometry techniques lack the sensitivity to characterize individual nanostructures. Although magnetic force microscopy (MFM) can be used to image the stray field above a sample, the technique is invasive and cannot be used to measure the magnetization within a sample quantitatively.

Here, we use off-axis electron holography[5] in the transmission electron microscope (TEM), in combination with micromagnetic simulations, to obtain quantitative information about the magnetic remanent states of adjacent, nominally identical 75×280-nm^2 pseudo-spin-valve structures, which were prepared from a polycrystalline $Ni_{79}Fe_{21}(4.1 \text{ nm})/Cu(3 \text{ nm})/Co(3.5 \text{ nm})/Cu(4 \text{ nm})$ film that had been sputtered onto an oxidized silicon substrate. A layer of tungsten was evaporated onto the film, followed by a trilayer resist stack, into which a pattern of rectangles was defined using interference lithography. This pattern was transferred into the tungsten using reactive ion etching, and then into the multilayer using ion milling.[6,7] The resulting structures were rectangular bars on a 280×770-nm^2 grid, covering an area of over a cm^2. The layout of the array of elements and the layer sequence within an individual element are shown schematically in Figs. 1(a) and 1(b), respectively.

II. EXPERIMENTAL DETAILS

A plan-view TEM sample preparation method based on focused ion-beam (FIB) milling with gallium was developed

---

[a]Author to whom correspondence should be addressed; electronic mail: tk305@cam.ac.uk
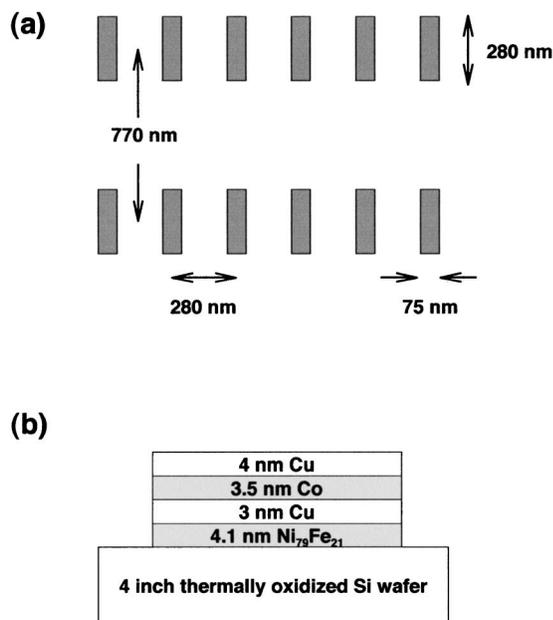
FIG. 1. Schematic diagrams showing (a) the layout of the rectangular array of pseudo-spin-valve elements, and (b) the nominal cross-sectional layer structure in each element.

in order to minimize the effect of sample preparation for electron microscopy on the magnetic properties of the elements. One corner of a small piece (a few mm^2) of the wafer was initially milled from the substrate side, parallel to the wafer surface, as shown in Figs. 2(a)–2(c), to produce an area of thermal oxide (not yet electron transparent) supporting a region of the magnetic elements. A hole was then formed in the middle of this membrane by ion milling from *below*, at a glancing angle to the wafer surface, as shown in Fig. 2(d). In this way, a part of the array of elements, which was located on the near side of the hole on an electron-transparent region of oxide, was protected from gallium ion damage during milling by the intervening substrate. The interior of the hole could also be used to provide a reference wave for electron holography. This approach proved to be highly successful for preparing a plan-view sample of un-damaged elements for electron holography, although some complications were encountered during ion milling as a result of charging of the thermal oxide. In contrast with conventional "trench" approaches used for FIB milling of samples for electron microscopy, a further advantage of preparing the electron-transparent region on a corner of the wafer was that sample tilt angles of up to ±60° could be achieved before this region was shadowed by other parts of the sample. Figure 3(a) shows a bright-field TEM image of a part of the area of interest on the final sample. It is apparent from Fig. 3(a) that only the very edge of the hole has been damaged by ion milling. The image shows that the elements have slightly different shapes, particularly at their ends, and are still partially coated with a small amount of residue, perhaps from lithography.

A Philips CM200-ST field-emission gun TEM was used to acquire electron holograms of the region of the sample shown in Fig. 3(a). Holograms were acquired at 200 kV using a (Lorentz) minilens, with the objective lens of the mi-
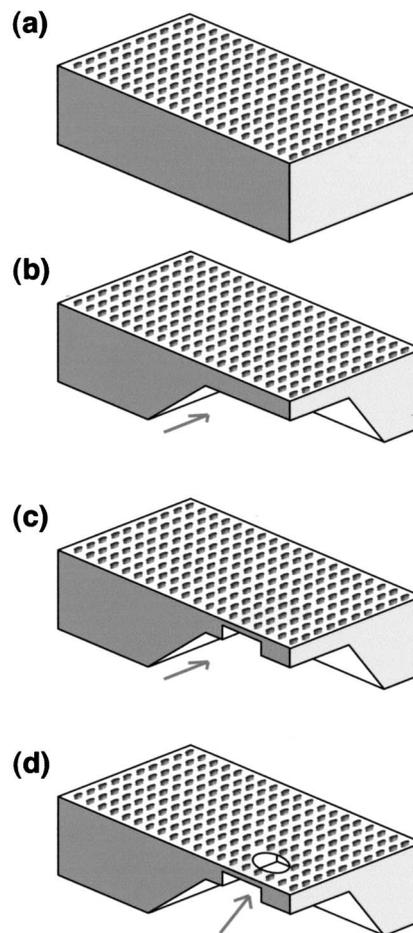

FIG. 2. Schematic diagrams illustrating the procedure used to prepare an electron-transparent plan-view sample of the pseudo-spin-valve elements for electron holography, by using focused ion-beam milling with gallium ions. (a) and (b) A piece of the original wafer is milled from the substrate side at one corner. (c) A membrane is formed that is parallel to the wafer surface but not yet electron transparent. (d) A hole is then formed in this membrane by milling from below, at a glancing angle to the original wafer surface. In this way, the elements that are on the near side of the hole are protected from ion damage and implantation by the intervening substrate, and the hole can subsequently be used to provide a reference wave for electron holography.

croscope switched off and the sample located in magnetic-field-free conditions. (The residual vertical magnetic field of the objective lens is estimated to be below 5 G.) The biprism voltage was 120 V, corresponding to an overlap width of 780 nm and a holographic interference fringe spacing of 4.4 nm, as shown in Fig. 3(b). Reference holograms were used to remove distortions associated with the imaging and recording system of the microscope. Eighteen holograms of three of the elements were acquired at remanence after saturating the sample magnetically either parallel or antiparallel to their length using the field of the conventional microscope objective lens, followed by applying a reverse field. All external fields were applied with the specimen tilted by ±30°, such that the out-of-plane component of the applied field was 1.73 times the in-plane component. The sample was always tilted back to 0° in zero field for electron holography, and imaged at remanence. In Fig. 3(b), the contrast of the holographic interference fringes, which is defined as $(I_{max}-I_{min})/(I_{max}+I_{min})$, where I_{max} and I_{min} are the maxi-
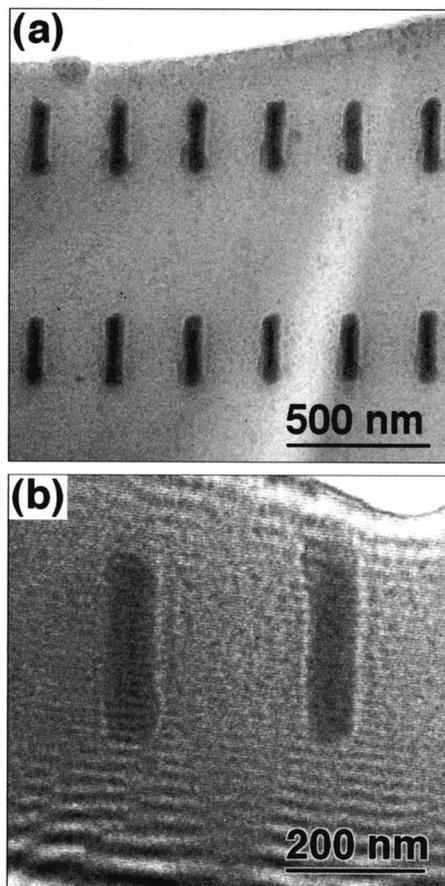
FIG. 3. (a) Plan-view bright-field transmission electron microscope image of part of the array of pseudo-spin-valve elements at the edge of the hole. (b) Part of a representative off-axis electron hologram of two of the elements in the array.
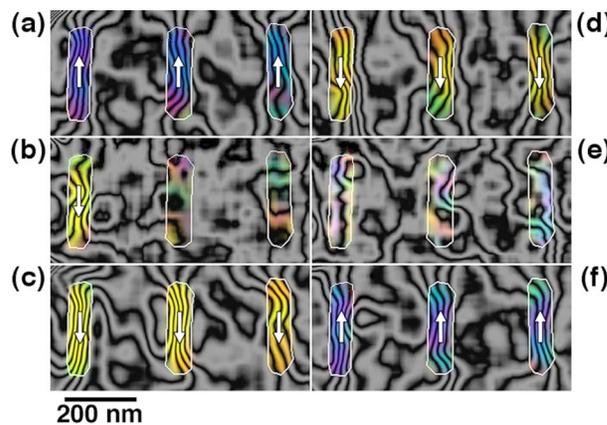

FIG. 4. (Color online) Experimental magnetic induction maps showing six different remanent magnetic states recorded using electron holography from three adjacent pseudo-spin-valve elements. Eighteen images similar to these were recorded in total. The outlines of the elements are shown in white. The contour spacing is $2\pi/64=0.098$ rad, such that the magnetic flux enclosed between any two adjacent black contours is $h/64e=6.25\times10^{-17}$ Wb. The direction of the magnetic induction in the elements is shown using arrows and according to a color wheel (red=right, yellow=down, green=left, and blue=up).

mum and minimum intensities of the fringes, respectively, are 1.9% in vacuum outside the specimen edge, 1.9% in the support film, and 1.2% in the elements. The remaining support film is estimated, from the holographic phase shift relative to vacuum, to have a thickness of approximately 43 nm close to the positions of the elements.

III. EXPERIMENTAL RESULTS

Figure 4 shows six representative magnetic induction maps of the three elements recorded using electron holography. Images (a)–(c) were acquired after saturating the elements upwards (in the plane of the page) and then applying external fields with in-plane components of (a) 0, (b) 424, and (c) 1092 Oe downwards. Images (d)–(f) were recorded after saturating the elements downwards and then applying external fields with in-plane components of (d) 0, (e) 317, and (f) 1092 Oe upwards. The contours were generated directly from the magnetic contribution to the measured holographic phase shift, after subtracting the mean inner potential (MIP) contribution from each recorded phase image, using a procedure that is described in detail elsewhere.[5] The contour spacing of $2\pi/64=0.098$ rad is inversely proportional to the in-plane component of the magnetic induction in the sample integrated in the electron-beam direction. Arrows have been added to elements in which the contours are closely spaced.

In these elements, the directions of the two magnetic layers are inferred to be parallel. In the remaining elements, in which the contours are widely spaced, the magnetic layers are inferred to be antiparallel. Detailed variations in the directions of the contours (particularly in the elements without arrows) are likely to be dominated by noise in the holograms. The spatial resolution of the contoured phase images shown in Fig. 4 is estimated to be approximately 15 nm.

Qualitatively, the images in Fig. 4 appear to show that the elements do not support end domains or vortices, and that there is little magnetic interaction between neighboring elements. However, in the absence of a substantial region of vacuum in the holograms it was necessary to add a slight phase ramp to each experimental phase image during analysis to compensate for slight drift of the biprism wire between acquiring the sample and reference holograms. The practical consequences of using this procedure, which is not usually required when imaging stronger magnetic fields, are discussed in detail below. The influence of demagnetizing fields on the results is also considered below.

Figure 5 shows a remanent hysteresis loop measured from the electron holographic phase images. The horizontal axis is the in-plane component of the magnetic field applied to the elements before recording the remanent states. The vertical axis is the step in the magnetic contribution to the phase shift across each element, measured from line profiles averaged over a distance of 70 nm parallel to the length of each element, after subtracting the MIP contribution to the phase shift. Each point is an average of such measurements obtained from the three elements shown in Fig. 4. The presence of clear steps in the loop confirms the formation of different remanent states: one with the layers aligned parallel and the other with the layers aligned antiparallel, as inferred in similar samples by using magnetometry[8] and MFM.[9] The two-step reversal in Fig. 5 is much better defined than that of Ni/Au/Co structures measured previously using electron holography.[10,11]
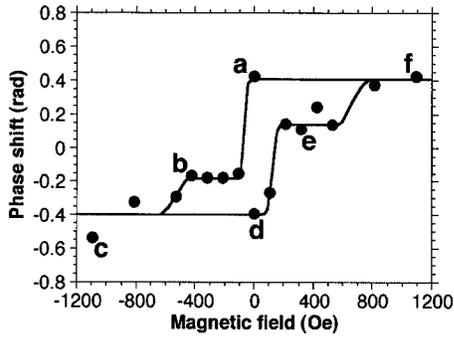
FIG. 5. Remanent hysteresis loop measured directly from the experimental electron holographic phase images, with the letters corresponding to the six individual figures shown in Fig. 4. The graph shows the magnetic contribution to the phase shift across each element, plotted as a function of the in-plane component of the field applied to the elements before recording the remanent states. Each point shows an average of the phase shifts measured from the three elements shown in Fig. 4.

The average switching fields of the three elements are approximately 100 Oe for the first layer to switch (assumed to be NiFe) and 600 Oe for the second layer to switch (assumed to be Co). The data points are spaced by ∼100 Oe, which limits the accuracy of the determination of the switching fields. The remanent loop is in reasonable agreement with the hysteresis data obtained using alternating-gradient magnetometry from ∼10^9 elements from another part of the same sample (Fig. 6). The average switching fields in Fig. 6 are −20 and 480 Oe for the two layers.

Electron holographic data from the three individual elements are shown in Fig. 7. The top graph (corresponding to the left element in Fig. 4) displays an antiparallel state in only one direction, with switching fields for the two layers of 100–200 and 100–400 Oe. In comparison, the other elements have switching fields of 100–200 and 500–700 Oe. Although the difference in the behavior of the three elements is surprising, switching variability in similar 70×550-nm elements has been observed previously using MFM.[9] In that experiment, NiFe switching fields in ten different elements ranged between 110 and 160 Oe, while Co switching fields ranged between 420 and 650 Oe. This variability is also seen in the collective hysteresis loop shown in Fig. 6, from which the switching field distributions of the NiFe and Co layers (measured as the half-width of a Gaussian fit to the derivative of the loop) are 50 and 150 Oe, respectively. The width of the switching field distribution is thought to result from variations in the shapes and sizes of the elements, which can
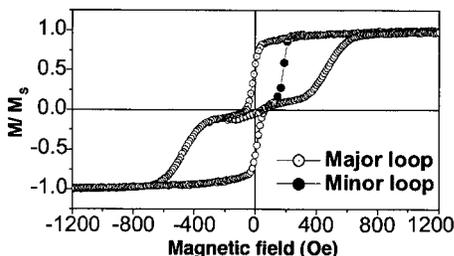

FIG. 6. Hysteresis loop measured by using magnetometry, from ∼10^9 elements on another region of the same sample. A minor loop is also shown. The vertical axis corresponds to the measured moment M as a fraction of the saturation moment M_S.
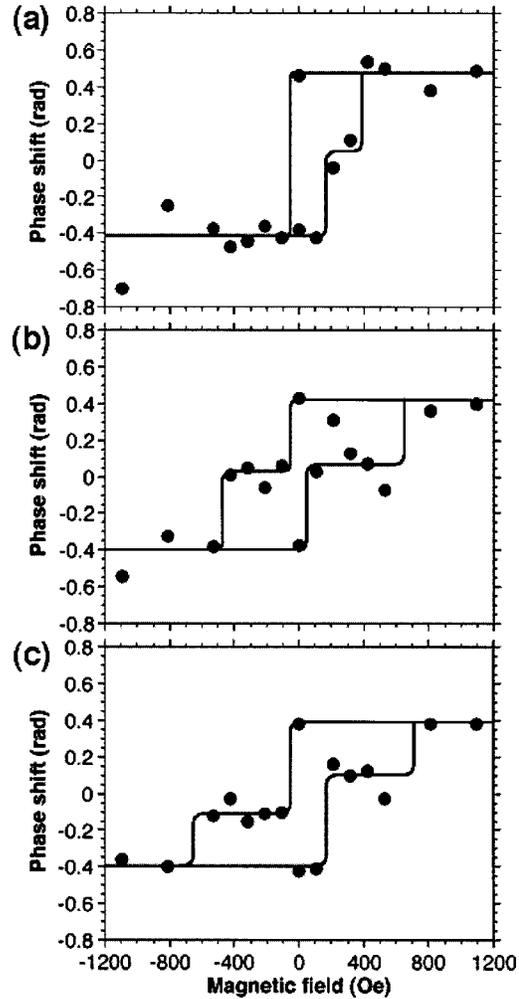

FIG. 7. Separate remanent hysteresis loops measured from each of the three elements shown in Fig. 4, illustrating the variability in both the switching field and the projected induction in the elements. The loops in (a)–(c) were obtained from the left, middle, and right elements, respectively, shown in Fig. 4.

be seen in Fig. 3(a), and from microstructural variability. The latter possibility is particularly important for the Co layer, in which a distribution of anisotropy axes of the polycrystalline Co grains can lead to a variable net anisotropy.

IV. MICROMAGNETIC SIMULATIONS

Unlike MFM, electron holography can be used to quantify the magnetic moments of the individual layers in the elements. If a pseudo-spin-valve element of width d were isolated, uniformly magnetized parallel to its length and infinitely long, then the step in the magnetic contribution to the phase shift across it would be given by the expression

$$\Delta\phi_{MAG} = \frac{e}{\hbar}d[B_2t_2 \pm B_1t_1], \tag{1}$$

where the in-plane component of the magnetic induction parallel to its axis is denoted B, the thickness of each layer t, the first and second layers to switch are denoted 1 and 2, respectively, the positive sign refers to parallel magnetic alignment of the layers, the negative sign to antiparallel alignment, e is the electronic charge, and $\hbar$ is Planck's constant h divided by

2π. By using values of $B_{Co}=1.8$ T (18 kG), $B_{NiFe}=1.0$ T (10 kG), $t_{Co}=3.5$ nm, $t_{NiFe}=4.1$ nm, and $d=75$ nm, and assuming that the NiFe layer switches first (see below), the phase shifts that would be predicted using Eq. (1) are +1.25 and +0.26 rad for the parallel and antiparallel states, respectively. In contrast, the averaged experimental loop in Fig. 5 shows a phase shift for parallel states of +0.4 rad, while antiparallel states have a phase shift of −0.15 rad. The negative value is particularly interesting, as it suggests that the first layer to switch is associated with a greater magnetic flux than the second, which is not expected either intuitively or from the nominal layer sequence if the NiFe layer switches first. Equation (1) cannot be used to address these discrepancies or to take the finite lengths and the demagnetizing fields of the elements into account. Micromagnetic simulations were therefore used to address these issues.

Simulations of magnetization reversal processes and magnetic remanent states in *isolated* pseudo-spin-valve elements were carried out by solving the Landau–Lifshitz–Gilbert equations in the continuum micromagnetic limit using LLG software.[12] (LLG simulations of rectangular arrays would have been computationally too intensive—the consequences of simulating only isolated elements are discussed below.) In each simulation, the element was modeled using discrete moments, with the demagnetization field computed to all orders. A gyromagnetic frequency γ of 17.6 MHz/Oe and a damping constant α of 1 were used, and the effects of thermal fluctuations were not included. The exit criterion for computing equilibrium magnetization distributions was triggered by the largest residual direction cosine of the moments in the grid changing by less than 10^{-4}. Saturation magnetizations of 800 and 1414 emu/cm^3, and exchange stiffnesses of 1.05 and 3.05 μerg/cm, were used for the NiFe and Co layers, respectively. As a result of the fine grain size in the elements, the magnetocrystalline anisotropy was set to zero in the ferromagnetic layers, which were separated by vacuum in the simulations. The simulations always incorporated both the in-plane and the out-of-plane components of the external field that were used in the electron holography experiments.

A simulated remanent hysteresis loop was fitted to the experimental results by varying the width and the length of the element, the thicknesses of the two ferromagnetic layers, and the spacing between them in the simulations. Figure 8 shows a simulated loop that is consistent with the experimental results, corresponding to an element with a length of 200 nm and a width of 38 nm, layer thicknesses of 4 nm for NiFe and 2 nm for Co, and a Cu layer thickness of 3 nm. Although the best-fitting simulation needs to be interpreted with care because the effects of microstructure and edge roughness, which may affect the coercivity of the element, have not been considered, the fitted parameters suggest that approximately 20 nm of material at the edge of the element does not contribute to the magnetic signal, in agreement with previous studies[13,14] that have indicated the presence of oxidized or amorphized material at the edges of ion-milled magnetic multilayer structures. Surprisingly, the Co layer also appears to be thinner magnetically than expected. However, electron holography only measures the magnetic flux in the plane of the elements, and the decrease in the measured phase shift
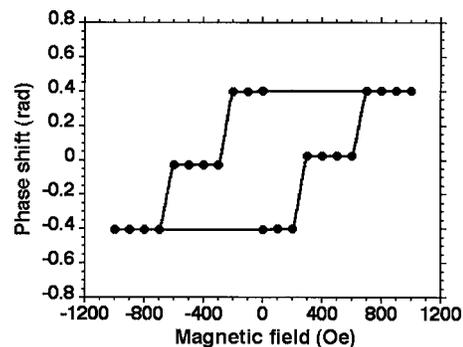

FIG. 8. Simulated remanent hysteresis loop of a single pseudo-spin-valve element that is in reasonable agreement with the experimental loops shown in Figs. 5 and 7. The phase images used to determine the loop were simulated using LLG micromagnetics software. The parameters used in the simulation were $t_{Co}=2$ nm, $t_{Cu}=3$ nm, $t_{NiFe}=4$ nm, $d=38$ nm, and the element length was 200 nm. In the simulations, all fields were applied to the element in the directions used for the experimental data (at angles of $\pm30°$ to the wafer normal).

may result from partial out-of-plane magnetization resulting from crystalline texture in the Co layer. (This possibility is difficult to address experimentally unless magnetic phase images are recorded as a function of specimen tilt angle.) The error in the fitted layer thicknesses that results from considering only an isolated element is discussed below. An important point to note from the simulations is that for the present elements the NiFe layer switches first unless it is more than 2.5 times thicker than the Co layer, and not 1.8 times thicker as might be expected from the ratio of magnetizations in the two layers. There is no evidence that the Co layer switches first in any of the experimental results reported here.

Corresponding phase contours for simulated magnetic remanent states are shown in Fig. 9 for the best-fitting parameters used to generate Fig. 8. The contour spacing is chosen to be four times smaller than in Fig. 4 in order to show variations in the spacing and direction of the simulated contours in detail. The contours in Fig. 9 are clearly curved at the ends of the elements. This curvature arises in part because the magnetization directions close to the ends of the elements are often not parallel to their length (see Fig. 10 below), but mostly because of the presence of demagnetizing
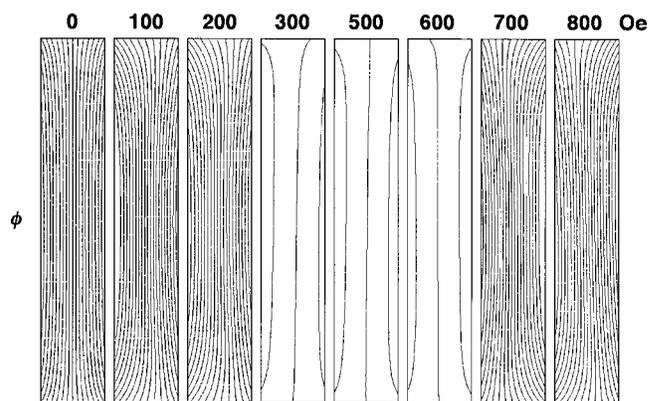

FIG. 9. Phase contours determined from the micromagnetic simulation used to calculate the remanent hysteresis loop shown in Fig. 8, for the values of applied field shown. The contour spacing is $2\pi/256=0.025$ rad. This is one-quarter of the contour spacing in Fig. 4.
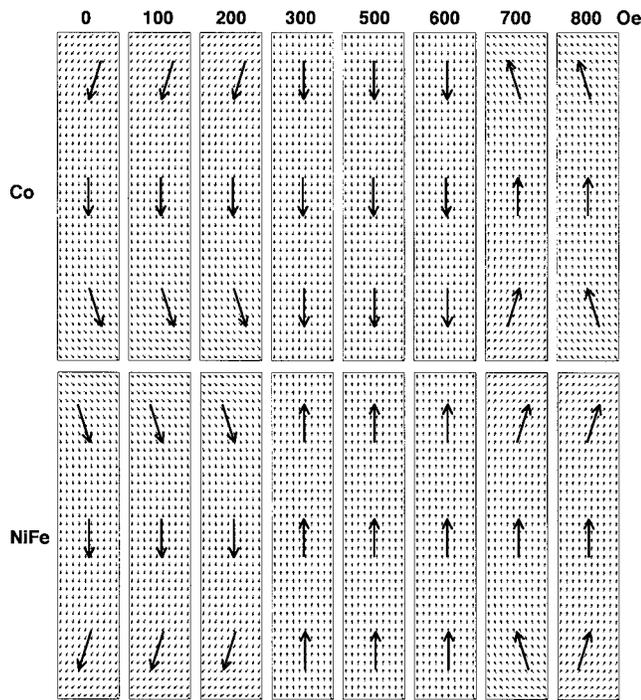
FIG. 10. Simulated magnetic induction in the Co and NiFe layers separately, during magnetization reversal of the spin-valve element described in Figs. 8 and 9, at the applied field values indicated.
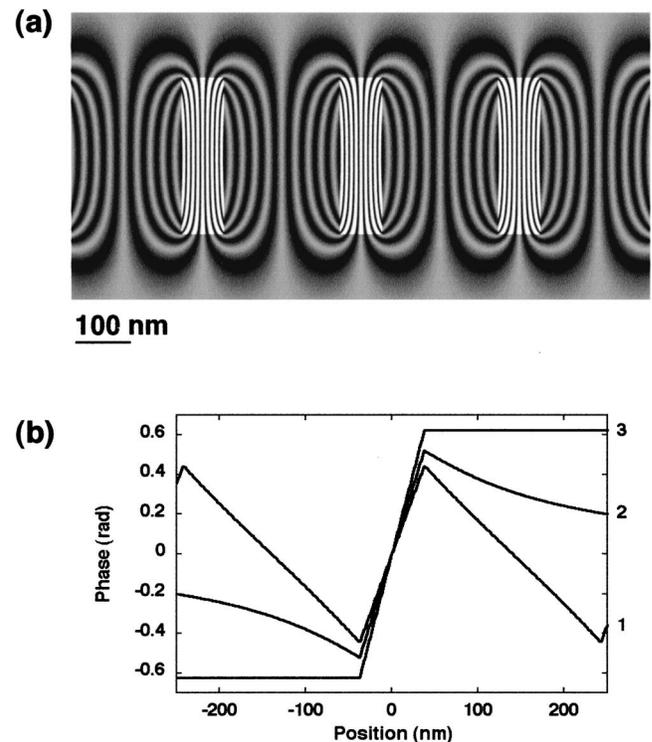

FIG. 11. (a) Simulation, calculated using the approach of Beleggia and Zhu (see Ref. 15), of magnetic phase contours for the nominal thicknesses, layer sequences, and separations of the elements, assuming that the Co and NiFe layers are saturated magnetically parallel to each other and to the length of each element. The contour spacing is $2\pi/64 = 0.098$ rad, as in Fig. 4. (b) Horizontal phase profiles across the centers of elements similar to those shown in (a), simulated for (1) the two-dimensional array of elements with a width of 75 nm and a length of 280 nm shown in (a); (2) one isolated element with a width of 75 nm and a length 280 nm; (3) one isolated element with a width of 75 nm and an infinite length. The magnetic contributions to the phase shift across the central element (the vertical range in each graph) are (1) 0.883, (2) 1.041, and (3) 1.248 rad.

fields. Figure 10 shows the details of the magnetization reversal process for the best-fitting parameters, in the form of vector maps of the magnetic induction in the Co and NiFe layers separately. It is apparent from the figure that the magnetic induction in the layers is only parallel to their length when they are magnetized in opposite directions. When they are magnetized in the same direction, they exhibit either *C* or *S* states, which are of opposite sense in the two ferromagnetic layers.

V. ARTIFACTS AND ERRORS

A possible source of error in the experimental measurements (other than statistical noise) is now considered. Figure 11(a) shows predicted phase contours both inside and outside pseudo-spin-valve elements for the nominal layer sequences and spacings, calculated using the Fourier space approach of Beleggia and Zhu[15] on the assumption that the Co and NiFe layers are saturated magnetically parallel to each other and to their length. The most surprising aspect of Fig. 11(a) is the prediction of a clear magnetic return flux between adjacent elements, which is absent from the experimental observations shown in Fig. 4. This discrepancy is likely to result from the approach that was used to analyze the electron holograms. If the magnetic contribution to a measured phase image is very weak, as in the present experiment, then a phase ramp may be present in an experimental phase image as a result of effects such as slight drift of the biprism wire between acquiring the sample and reference holograms. This artifact can only be measured experimentally if a substantial region of vacuum is present in each recorded hologram. It is instead usually removed by manually adding a phase ramp to the experimental image until a contour map that is physically

reasonable is obtained. In the present experiment, the number of phase contours within each element is likely to have been maximized by using this approach, resulting in an artificial and incorrect cancellation of the demagnetizing field between the elements and a consequent small error in the measurements of phase shifts across them.

A horizontal phase profile obtained from the image used to calculate Fig. 11(a), drawn through the center element, is shown as line 1 in Fig. 11(b). Equivalent simulations for a single isolated element of the same size (line 2) and a similar element that has infinite length (line 3) are also shown. Line 3 is consistent with the phase shift across a single element of 1.25 rad that would be calculated on the basis of Eq. (1). The demagnetizing field of an isolated element reduces the phase shift across it to 83% of this value (line 2), while the demagnetizing fields of all of the elements in the rectangular array reduce it to 71% (line 1). The difference between the phase shifts determined from lines 2 and 3 provides an indication of the error in the fitted layer thicknesses and/or widths introduced by considering an isolated element, rather than an array, in the LLG simulations described above. This error corresponds to an underestimate of the product of the magnetic layer thickness and width of up to 17%. The effect of adding a ramp to the phase image used to generate Fig. 11(a) is
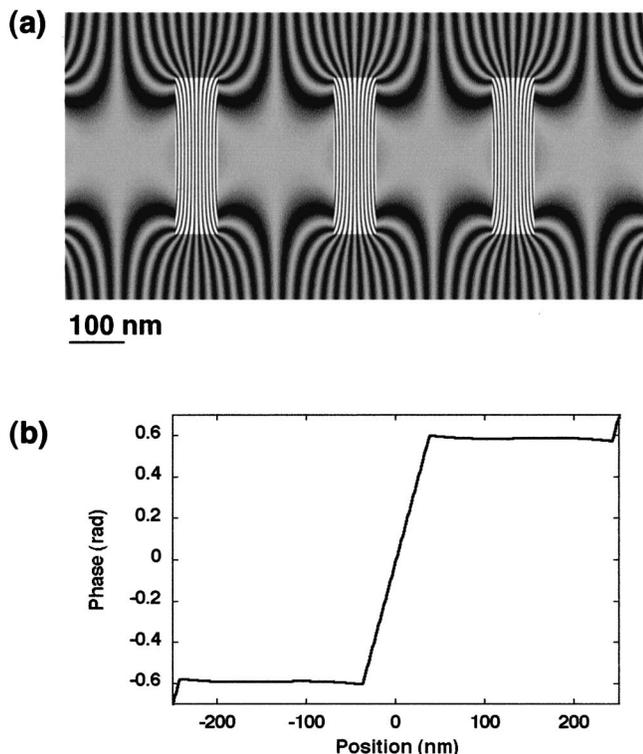
(a)

100 nm

(b)

FIG. 12. (a) As for Fig. 11(a), but now after adding a phase ramp to the simulation before forming the contours, in order to artificially remove the magnetic return flux between the elements. (b) Horizontal phase profile obtained from the phase image used to generate (a). The magnetic contribution to the phase shift across the central element (the vertical range in the center of the graph) is 1.204 rad.

shown in Fig. 12(a). By adding a ramp, it is possible to generate closely spaced contours above and below each element that are similar to those seen experimentally in Fig. 4, with little return flux visible between the elements. Paradoxically, the step in phase, which is shown in Fig. 12(b), is now very close to the prediction of Eq. (1). When considered together with the use of an isolated element in the LLG simulations, the practical consequence of carrying out this procedure is that the products of the magnetic thicknesses and the widths of the NiFe and Co layers may be overestimated by approximately 17% in the best-fitting remanent hysteresis loop shown in Fig. 8. For example, if the fitted layer widths are correct, then better estimates of the magnetic thicknesses of the NiFe and Co layers are 3.3 and 1.7 nm, respectively.

VI. SUMMARY AND CONCLUSIONS

Quantitative information about magnetic remanent states in Co/Cu/NiFe thin-film elements has been obtained using electron holography. Separate switching of the Co and NiFe layers in individual elements has been identified, and the remanent states have been shown to exhibit near-uniform magnetization configurations. The magnetic signal is lower than would be predicted from the nominal layer thicknesses. Micromagnetic simulations suggest that approximately 20 nm of material at the edge of each element may not contribute to the magnetic signal, possibly as a result of oxidation or amorphization during sample fabrication. In addition, the in-plane component of the magnetic induction in the Co layer is reduced by at least 40% from its nominal value. Significant differences in the measured hysteresis behavior of three adjacent elements are thought to result from shape and microstructural variations. This variability must be minimized if such elements are to be used in ultrahigh areal density magnetic recording applications.

[1] S. S. P. Parkin *et al.*, J. Appl. Phys. **85**, 5828 (1999).
[2] R. Katti, J. Appl. Phys. **91**, 7245 (2002).
[3] M. Saito *et al.*, IEEE Trans. Magn. **40**, 207 (2004).
[4] K. B. Klaassen, X. Xing, and J. C. L. van Peppen, IEEE Trans. Magn. **40**, 195 (2004).
[5] R. E. Dunin-Borkowski, M. R. McCartney, and D. J. Smith, *Encyclopaedia of Nanoscience and Nanotechnology*, edited by H. S. Nalwa (American Scientific, New York, 2004), Vol. 3, pp. 41–100.
[6] B. Vogeli, H. I. Smith, F. J. Castaño, Y. Hao, S. Haratani, and C. A. Ross, J. Vac. Sci. Technol. B **19**, 2753 (2001).
[7] C. A. Ross *et al.*, J. Appl. Phys. **91**, 6848 (2002).
[8] F. J. Castaño, Y. Hao, M. Hwang, C. A. Ross, B. Vogeli, H. I. Smith, and S. Haratani, Appl. Phys. Lett. **79**, 1504 (2001).
[9] X. Zhu, P. Grutter, Y. Hao, F. J. Castaño, S. Haratani, C. A. Ross, B. Vogeli, and H. I. Smith, J. Appl. Phys. **93**, 1132 (2002).
[10] D. J. Smith, R. E. Dunin-Borkowski, M. R. McCartney, B. Kardynal, and M. R. Scheinfein, J. Appl. Phys. **87**, 7400 (2000).
[11] R. E. Dunin-Borkowski, M. R. McCartney, B. Kardynal, S. S. P. Parkin, M. R. Scheinfein, and D. J. Smith, J. Microsc. **200**, 187 (2000).
[12] http://llgmicro.home.mindspring.com/
[13] F. J. Castaño, S. Haratani, Y. Hao, C. A. Ross, and H. I. Smith, Appl. Phys. Lett. **81**, 2809 (2002).
[14] J. A. Katine, M. K. Ho, Y. S. Ju, and C. T. Rettner, Appl. Phys. Lett. **83**, 401 (2003).
[15] M. Beleggia and Y. Zhu, Philos. Mag. **83**, 1045 (2003).